Supporting Information

Ultra-uniform high-quality plasmonic metasurfaces through electrostatic self-assembly of gold nanoparticles on chemically unmodified glass

Adriano Acunzo[1,2], Maria De Luca[1], Daniele Marra[1], Bartolomeo Della Ventura[1], Andreas Offenhäusser[2], Dirk Mayer[2] and Raffaele Velotta[2]**

[1]Department of Physics *Ettore Pancini*, University of Naples Federico II, Via Cintia 26, 80126 Naples, Italy.

[2]Institute of Biological Information Processing (IBI-3), Bioelectronics, Forschungszentrum Jülich, 52425 Jülich, Germany.

*E-mail: dirk.mayer@fz-juelich.de, *rvelotta@unina.it.

Table of contents

1.1. Synthesis of gold nanoparticles

Initial CTAB-capped Gold Seeds

The initial CTAB-capped seeds for AuNRs were synthesized according to Mirkin's paper[1], with integrations from El-Sayed's seminal paper.[2] Firstly, 5 mL of 100 mM CTAB was warmed at 28°C under gentle stirring till complete solubilization (solution color: transparent), 100 mM being the maximum solubility of CTAB in water at 20°C. Afterwards, 125 µL of 10 mM $HAuCl_4$ were added and thoroughly mixed for 2 min under vigorous stirring. At this stage, the solution color turned from transparent to a characteristic dark yellow due to the $AuCl_4^-$ adsorption to CTAB micelles.[3] Finally, 300 µL of freshly prepared ice-cold 10 mM $NaBH_4$ was rapidly injected and vigorously stirred for 2 min. Then, stirring was stopped, magnetic rod removed, and solution kept at 25 °C (to avoid CTAB crystallization) until NRs synthesis. It is indeed recommended to age the seed solution for 2-6 h prior to use to allow for complete hydrolysis of unreacted $NaBH_4$.[4] Seed solution was not stored nor used beyond this time period since it degrades during time: its initial light yellow-brown color slowly turned to light pink over a week, signaling the formation of larger AuNPs. It is also worth stressing that $NaBH_4$ powder should be freshly prepared for every synthesis, dissolved in ice-cold ultrapure water (rather than in room-temperature water to be refrigerated afterwards), and used as soon as possible. In fact, $NaBH_4$ separates into Na^+ and BH_4^- once in water, and BH_4^- is soon hydrolyzed (with release of H_2 pressurizing the vial). Since BH_4^- is the actual reducing specie for the seeds formation, its hydrolysis is an unwanted process to be limited as mentioned above.

Gold Nanorods (AuNRs)

Following again the synthesis of Mirkin's and El-Sayed's papers, 130 mL of 100 mM CTAB was first warmed to 28°C under gentle stirring until fully dissolved. Then, 6.5 mL of 10 mM

$HAuCl_4$ was added and mixed for 2 min under vigorous stirring. At this stage, the solution exhibited a characteristic dark yellow color due to $AuCl_4^-$ adsorption onto CTAB micelles.[3] Then, 1.17 mL of freshly prepared 10 mM $AgNO_3$ and 741 µL of freshly prepared 100 mM L-ascorbic acid were added in succession and stirred for 2 min each. The addition of L-ascorbic acid changed the solution color from dark yellow to transparent, as Au^{3+} is reduced to Au^+. The as-obtained solution served as growth solution for AuNRs. Indeed, 156 µL of freshly prepared initial gold seeds (see previous protocol) were finally added to the growth solution (at 28 °C) and thoroughly mixed under vigorous stirring for 2 min. Subsequently, stirring was stopped, magnetic rod removed, and the solution left untouched in the 28°C water bath for 2 h (to let the AuNRs grow). At this time, AuNRs usually exhibited OD 1.3 ± 0.1 at the l-LSPR of 700 ± 5 nm. Growth process was stopped, and excess of reagents removed, by 2 rounds of centrifugations and resuspensions by 50 mM CTAB each time. The parameters used for centrifugation were (4300 g, 15 min, RT) at Eppendorf MiniSpin® (max rotor radius: 6 cm), or (6300 g, 30 min, RT) at Heraeus Megafuge 1.0 R (max rotor radius: 15.5 cm). In view of the next step, AuNRs concentration was brought to OD 2 by adding 50 mM CTAB as well.

Final CPC-capped Gold Seeds

The final CPC-capped gold seeds were obtained from the AuNRs oxidative dissolution first reported by Liz-Marzán.[3] We followed both Liz-Marzán's and Mirkin's papers.[1,3] A desired amount of AuNRs at OD 2 in 50 mM CTAB was brought to a final concentration of 90 µM $HAuCl_4$ by adding a suitable volume of 10 mM $HAuCl_4$, keeping the solution under gentle stirring for 4 h at 40°C. At this point, the etched NPs usually exhibited OD 0.25 ± 0.05 at the LSPR of 524 ± 1 nm. The dissolution process was stopped, and excess of reagents removed, by (at least) 3 rounds of centrifugations and resuspensions by 100 mM CPC each time. This step

was essential to remove residues of CTAB and gold leading to unwanted dissolutions in the next steps. Roughly, CTAB content was dropped down to nM level. The parameters used for centrifugation were (8100 g, 30 min, RT) at Eppendorf MiniSpin® (max rotor radius: 6 cm). In view of the next synthesis, the concentration of the colloidal solution was brought to OD 1 by adding 100 mM CPC. The colloid was stored at room temperature until use up to 4 weeks. No measurable changes in UV-Vis spectrum were observed over this time period.

Gold Concave Rhombic Dodecahedra (AuCRD)

AuCRD were synthesized according to the works of Niu[5] and Mirkin[1]. 20 mL of 10 mM CPC was warmed at 25°C under gentle stirring. Then, 350 µL of 10 mM $HAuCl_4$ and 4.5 mL of freshly prepared 100 mM L-ascorbic acid were added in succession and thoroughly stirred for 2 min each. The addition of gold turned the solution color from transparent to dark yellow while the subsequent addition of L-ascorbic acid turned the color back to transparent. The as-obtained solution served as growth solution for the AuCRD. A desired amount of seeds adjusted to yield a desired AuCRD size (typically, 100-200 µL of seeds at OD 1 and 100 mM CPC) was then injected in the growth solution and thoroughly mixed under vigorous stirring for 1 min. Subsequently, stirring was stopped, magnetic rod removed, and the solution left untouched in the 25°C water bath for 30 min (to let the CRD grow). Growth process was stopped, and excess of reagents removed, by 3 rounds of centrifugations and resuspensions. Ultrapure water was used as buffer for the first resuspension while 50 mM CTAB for each of the remaining two resuspensions. The initial use of ultrapure pure (rather than CTAB) avoids undesired AuCRD dissolutions at this stage, due to residues of unreacted gold in the growth solution (even ≤0.1 µM $HAuCl_4$ triggered dissolution in presence of 50 mM CTAB). The parameters used for centrifugations were (150 g, 15 min, RT) at Eppendorf MiniSpin® (max rotor radius: 6 cm), or (500 g, 30 min, RT) at Heraeus Megafuge 1.0 R (max rotor radius: 15.5 cm). In view of the

subsequent dissolution to NSs, AuCRD concentration was brought to OD 1 by adding 50 mM CTAB as well. The above protocol was found to be scalable up to a factor 10 in volume, at least. Many sizes of AuCRD could be synthesized according to this protocol: the lower the amount of seeds, the larger the size of AuCRD. In particular, AuCRD140 were synthesized by the addition of 140 μL of seeds (at OD 1 and 100 mM CPC) to the growth solution.

Gold Nanospheres (AuNSs)

AuNSs (AuNS140) were obtained from oxidative dissolution of AuCRD140.[1,3] The desired amount of AuCRD140 at OD 1 in 50 mM CTAB was brought to a final concentration of 20 μM $HAuCl_4$ by adding a suitable volume of 10 mM $HAuCl_4$, keeping the solution under gentle stirring for 4 h at 40°C. Dissolution process was stopped, and excess of reagents removed, by 2 rounds of centrifugations and resuspensions by 0.5 mM CTAB each time. The parameters used for centrifugation were (150-250 g, 20 min, RT) at Eppendorf MiniSpin® (max rotor radius: 6 cm) and (500 g, 30 min, RT) at Heraeus Megafuge 1.0 R (max rotor radius: 15.5 cm). It is worth noting that CTAB concentration of 0.5 mM is lower than its critical micelle concentration of 0.9 mM,[6] hence no further dissolutions may take place during storing.

Gold Nanocubes (AuNCs)

Gold nanocubes (AuNCs) were synthesized according to the works of Niu[5] and Mirkin.[1] 5 mL of 100 mM CPC were warmed at 30°C under gentle stirring. Then, 500 μL of 100 mM KBr, 100 μL of 10 mM $HAuCl_4 \cdot 3H_2O$, and 150 μL of 100 mM L-ascorbic acid were added in succession and thoroughly mixed under vigorous stirring for 1 min each. The as-obtained solution served as growth solution for the NCs. In particular, 60 μL of seeds at OD 1 and 100 mM CPC were typically injected in the growth solution and thoroughly mixed under vigorous stirring for 1 min. Subsequently, stirring was stopped, magnetic rod removed, and the solution left untouched in the 30°C water bath for 1 h (to let the AuNCs grow). Growth process was

stopped, and excess of reagents removed, by 2 rounds of centrifugations and resuspensions by 1 mM CPC. The parameters used for centrifugations were (200–400 g, 15 min, RT) at Eppendorf MiniSpin® (max rotor radius: 6 cm), or (600–1000 g, 30 min, RT) at Heraeus Megafuge 1.0 R (max rotor radius: 15.5 cm). The above protocol was found to be scalable and reproducible up to a factor 20 in volume, at least. Many sizes of AuNCs could be synthesized according to this protocol by adjusting the amount of seeds in the range 50 – 150 μL: the lower the amount of seeds, the larger the size of AuNCs. In this regard, it is worth mentioning that surfactant-related depletion forces[7–9] induced *reversible* clustering of the AuNCs obtained by ≤100 μL seeds during the synthesis itself. This process gradually turned the colloid color to grey, with corresponding extinction spectrum exhibiting an almost horizontal line modulated by two wide plasmon peaks. However, the AuNCs clusters were *reversible* and fully disrupted as soon as the CPC concentration was lowered at 1 mM after the first round of centrifugation and resuspension.

1.2. Fabrication of gold nanoparticles ultra-uniform metasurfaces

The fabrication generally counted six steps:

1. Freshly synthesized AuNSs (AuNSs140) and AuNCs (AuNCs60) were centrifuged and resuspended at least 3 times using 0.5 μM CTAB and CPC buffer solutions, respectively. The colloids were then brought to a final OD 5 by further diluting with the corresponding buffers. For centrifugations at Eppendorf MiniSpin® (max rotor radius: 6 cm), AuNSs were centrifuged by (≈150 g, 15', RT) while AuNCs by (≈220 g, 15', RT). At Heraeus Megafuge 1.0 R (max rotor radius: 15.5 cm), both AuNSs and AuNCs (≤20 mL in 50 mL tubes) were centrifuged by (≈700 g, 30', 25°C).
2. 24×60 mm or 24×32 mm Menzel-Gläser nr.1 glass coverslips (D263M colorless borosilicate glass) were cleaned in an ultrasonic bath for 5 min by pure isopropyl alcohol and ultrapure water sequentially. Afterwards, the glass substrates were rinsed by ultrapure water and dried by a gentle stream of nitrogen.
3. The cleaned glass substrates were activated by a low-pressure oxygen plasma (0.8 mbar, 200 W, 5') at Diener Electronic PICO low-pressure plasma system, to increase the silanol bonds serving as (electrostatic) bonding sites for the positively charged CTAB-capped AuNSs and CPC-capped AuNCs.
4. The activated glass substrates were incubated for 4 h at room temperature by 2 mL of AuNSs or AuNCs at OD 5 and 0.5 μM CTAB or CPC (prepared as in a)). In particular, the colloidal solutions were directly pipetted onto the top surfaces of the glass coverslips (placed in a petri dish), thus avoiding an undesired nanoparticle deposition onto the bottom glass surfaces.
5. After 4 h, ultrapure water was used to thoroughly rinse the fresh AuNPs metasurfaces and remove unbound NPs. This step was carried out by keeping the metasurfaces soaked in the

liquids (in a petri dish) and replacing ultrapure water several times. Then, ultrapure water was slowly exchanged by a 5% isopropyl alcohol aqueous solution added dropwise. Finally, the metasurfaces were rapidly dried by a vigorous stream of nitrogen (≈3 bars). Solvent exchange and fast drying reduced surface tensions and capillary forces, minimizing morphological alterations of the fresh AuNPs metasurfaces (*e.g.*, NPs drifts, clusters formation) associated with an unproper drying (see section S5).

6. The AuNPs metasurfaces were cleaned from CTAB or CPC ligands through a low-pressure oxygen plasma treatment at Diener Electronic PICO low-pressure plasma system, leaving the bare AuNPs anchored to the bare glass substrate. AuNSs metasurfaces were treated by (0.8 mbar, 200 W, 30'); instead, AuNCs metasurfaces by (0.8 mbar, 200 W, 3') to prevent plasma-induced modifications of the cubic shape.

Apparently, the set of deposition conditions included four factors critical for high surface density: surfactant concentration, salt concentration (i.e., the ionic strength), nanoparticle concentration (i.e., the OD of the AuNPs colloids) and deposition time. However, as discussed in the main, surfactants and salts concentrations had to be constrained at very low levels to allow nanoparticle deposition and prevent clustering, respectively. Considering that the AuNPs colloids were found to be unstable at ≈ 0.25 μM CTAB/CPC, we fixed the surfactants concentrations at 0.5 μM. On the other hand, the salts concentrations were nominally zero, *i.e.*, trace residues after the multiple centrifugation and resuspensions steps. This implied that only the latter two factors were actually free parameters. Following a common procedure in nanoparticles self-assembly, in few preliminary experiments we progressively increased both the ODs of the AuNPs colloids and the incubation times (while keeping fixed the first two parameters), and found no measurable

increase in the surface densities for $OD > 5$ and incubation times $\Delta t > 4h$. Since the plasmon phenomena of LSPR blueshift and narrowing became more and more obvious for denser and denser metasurfaces, we eventually focused our efforts on the densest metasurfaces, fabricated through the deposition of AuNPs colloids at OD 5, 0.5 μM CTAB/CPC, and ≈ 0 μM salts for 4 h.

As already remarked in the main, the solvent exchange procedure worked equally well when employing a 5% ethyl alcohol (EtOH) aqueous solution, owing to the similar physicochemical properties of EtOH and IPA. In contrast, the procedure failed when using pure or concentrated IPA or EtOH aqueous solution (e.g., 50% IPA or EtOH), as the AuNPs detached from the glass substrate during either the solvent exchange or the drying step. This behavior was attributed to the higher solubility of CTAB and CPC surfactant molecules in concentrated IPA and EtOH solutions compared to dilute solutions or water, which likely facilitated their desorption from the surfaces of the surfactant-capped AuNPs previously immobilized on the substrate. The resulting reduction in the AuNPs positive surface charge, conferred by the surfactant capping layer, may readily account for their detachment under these different solvent conditions

S1. Morphological analysis of AuNSs

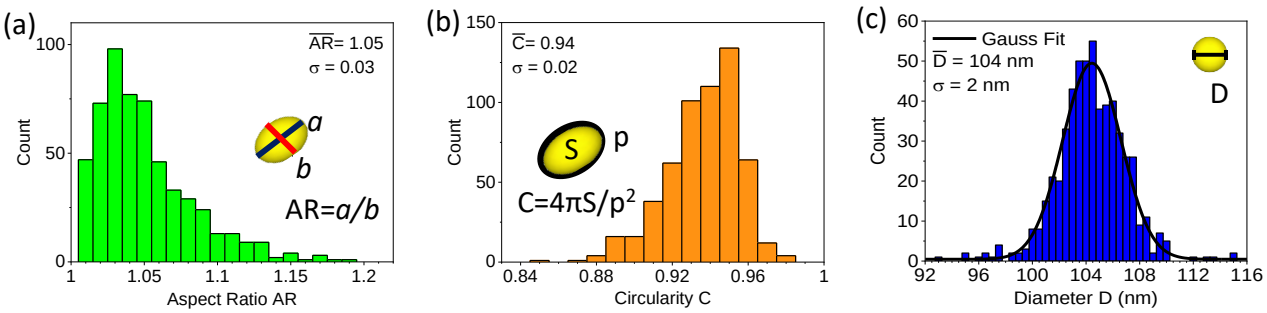

Figure S1. (a) Histogram of AuNSs aspect ratio (*AR*), with the inset representing the major (dark blue) and minor (red) axis of an idealized ellipsoid. (b) Histogram of AuNSs circularity (*C*), with the inset showing an idealized ellipsoid decomposed in perimeter (black line) and area (yellow filling). (e) Histogram of AuNSs sputtered-corrected diameter (*D*) distribution and its Gaussian fit. The sample investigated counts the 567 NPs from the STEM micrograph of Figure 2b.

S2. Thickness of the iridium sputtering layer

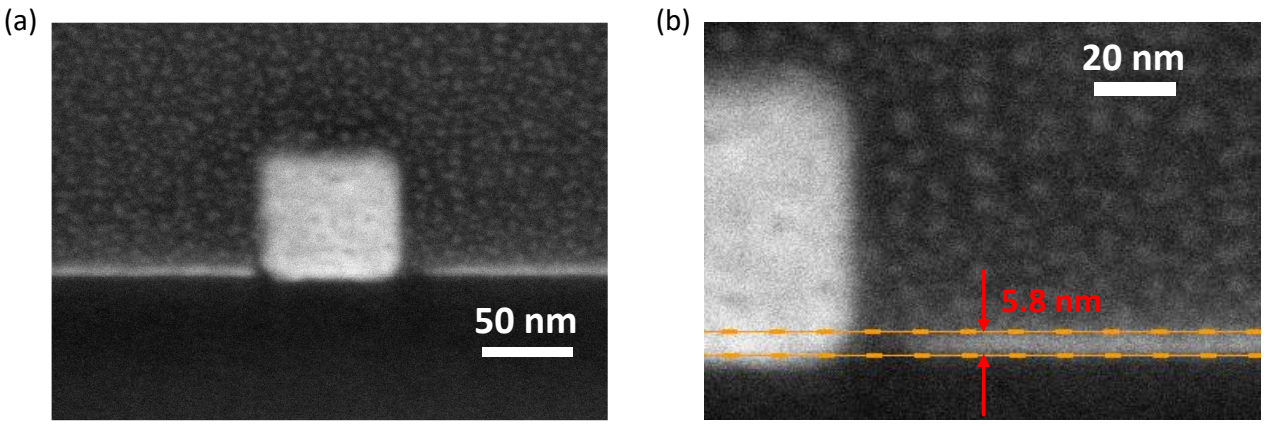

Figure S2. STEM micrographs of a Focused Ion Beam (FIB) cross section of a AuNCs metasurface on glass, showing one AuNC and the iridium sputtering layer resulting from the (60 s, 25 mA) sputtering process. (a) Overall image, exhibiting a uniform iridium layer. (b) Right side of the previous image, reporting the measurement of the iridium layer thickness by ImageJ.

S3. Morphological analysis of AuNCs: rectangular shape and size

After binarization and segmentation, the "Oriented Bounding Box" tool from the ImageJ "MorphoLibJ" plugin was employed to retrieve the lengths of both sides of the visible NPs. This tool considers as "length" (L*) and "width" (W*) the major and minor sides of the oriented

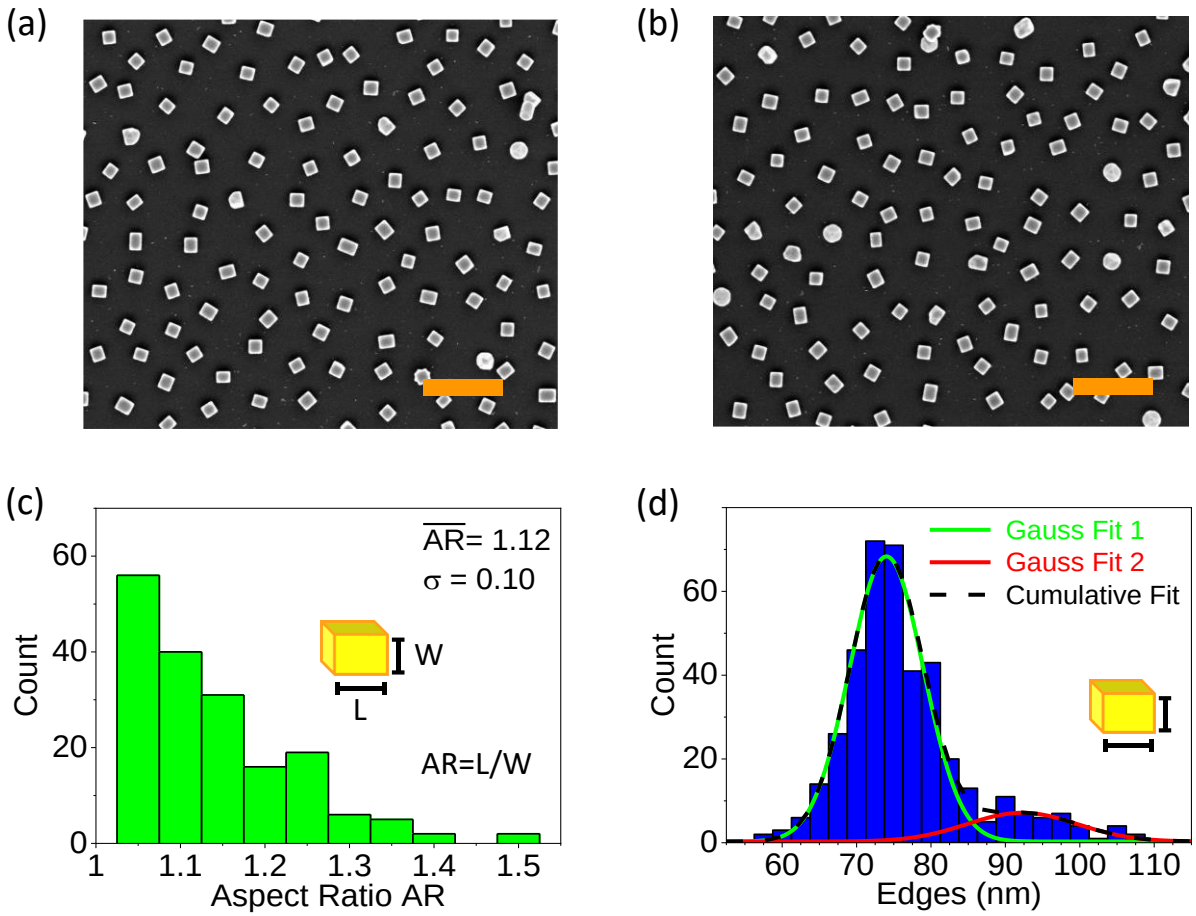

Figure S3. (a, b) Top-view STEM micrographs considered for this analysis, counting 200 NPs. Scale bars: 500 nm. (c) Histogram of AuNCs aspect ratio, the inset representing major (L) and minor (W) edges of an idealized parallelepiped. (d) Histogram of the sputtering- and artifact-corrected AuNCs edges with Gaussian fits for ordinarily grown edges (green), overgrown edges (red) and entire sample (dashed black). See the text for details on processing and analysis.

rectangle bounding an object, respectively. Since this rectangle bounds an object from the outside, L* and W* are slight overestimations of the actual length (L) and width (W) of the

visible object. In fact, the bounding box includes *all* the pixels of an object; in particular, it includes all the pixels along the object outline, which is not smooth because of the finite resolution of a micrograph, processing steps, etc. It follows that L^* and W^* are upper limits for the actual length L and width W of a rectangular object. The overestimation was manually checked to be within 3 nm for the considered micrographs, and this value sums to the $6 + 6 = 12$ nm associated with the iridium sputtering. To conclude, the actual length and width were estimated as $L = L^* - (3 + 12)$ nm and $W = W^* - (3 + 12)$ nm. These latter values of L and W were used for the analysis shown in Figure S3.

S4. Morphological analysis of AuNCs: corners curvature

A methodical analysis was conducted to estimate the mean radius of curvature $\overline{R_{curv}}$ for the visible corners of AuNCs (Figure S4a). The top–view STEM micrograph at high magnification (250'000x) of Figure S4b was analyzed at this scope, counting a sample of 68 corners from 19

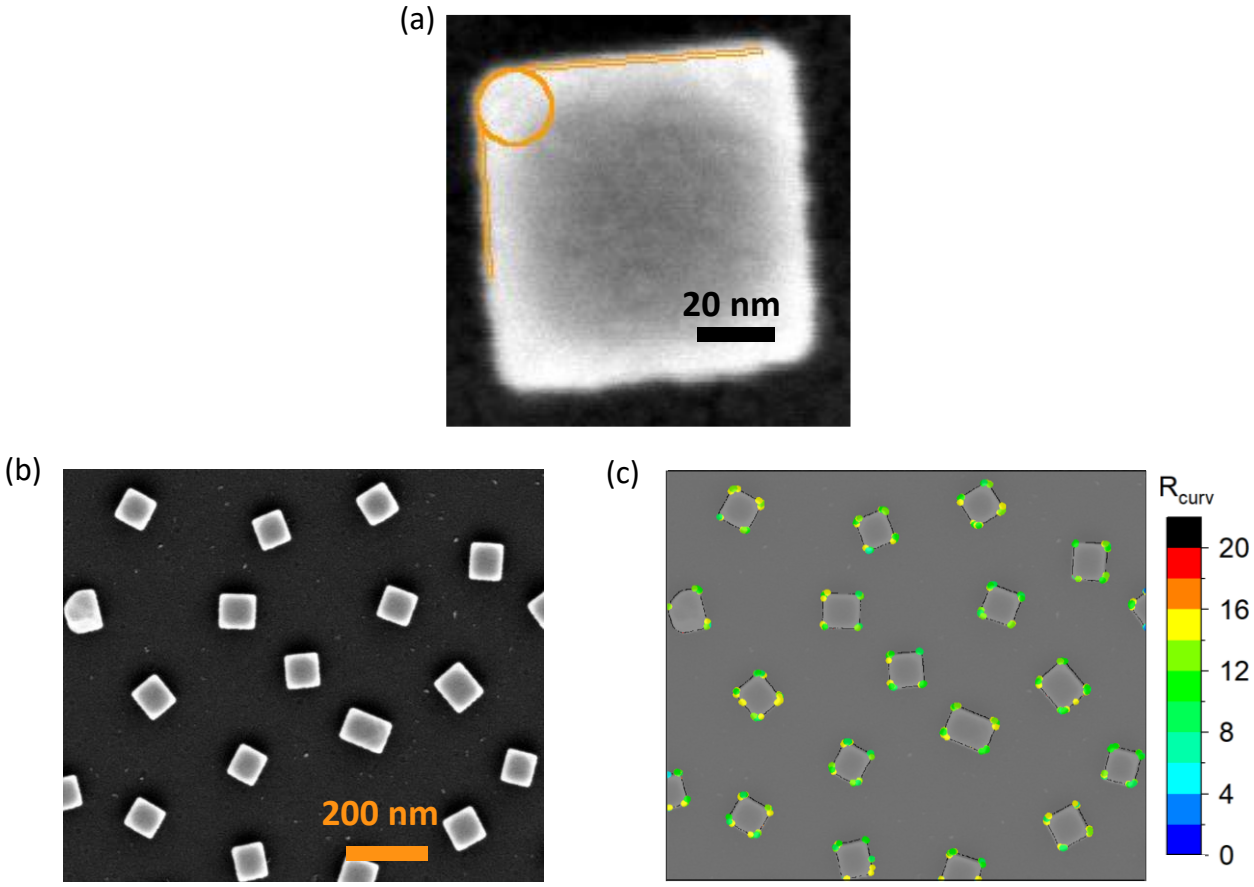

Figure S4. (a) Top-view STEM micrograph at high magnification (500'000x) showing one AuNC (the one at the center of the micrograph (b)). The orange circle has a radius of 10 nm, as resulting from the analysis of this specific corner. (b) Top-view STEM micrograph at high magnification (250'000) of a AuNCs metasurface together with (c) the graphical representation of the corresponding corner curvatures R_{curv}. The graph is superimposed onto the micrograph. For better readability, only coloured dots corresponding to R_{curv} in the range]0, 16[(blue to yellow) are displayed. Points with higher R_{curv} mostly lie beyond the corner regions.

NCs (few corners are outside the image). The ImageJ "Curvature" plugin was employed to list

the radius of curvature $R_{curv}(x, y)$ of each point (x, y) from the NPs outlines, with each local minimum corresponding to a corner. All points in the neighbourhood of a local minimum were considered till a discontinuity $\gtrsim 5$ nm in R_{curv} was encountered (excluding such discontinuous points). For each corner, the selected range was averaged, obtaining the mean radius of curvature ${R_{curv}}^{i}$ of that specific corner. Finally, we assumed all corners as independent and obtained $\overline{R_{curv}} = 12$ nm with standard deviation $\sigma = 2$ nm. Figure S4c displays a graphical representation of the raw data provided by the "Curvature" plugin. The graph is superimposed to the corresponding micrograph of Figure S4b and, for a better readability, points with $R_{curv} > 16$ nm are not represented (they mostly lie beyond the corner regions). It can be noted that the dominating colors at the corners are green and yellow, corresponding to points with R_{curv} from 8 to 16 nm. It is worth to stress that $\overline{R_{curv}} = 12 \pm 2$ nm refers to visible edges strictly, as a top-view micrograph cannot give information about the 3D curvature of vertices (which are truncated). However, we assumed $\overline{R_{curv}}$ as the radius of curvature of the entire corner. The result $\overline{R_{curv}} = 12 \pm 2$ nm indicates that the corners of our AuNCs are sharp, even though not super sharp. In fact, radii of curvature as small as 8.27 ± 0.39 were estimated (by ImageJ) from TEM micrographs of 72 nm AuNCs synthesized by a different protocol with optimized bromide concentration,[10] even though the authors did not describe their analysis method in detail.

S5. Effects of an unproper drying on the metasurfaces morphology

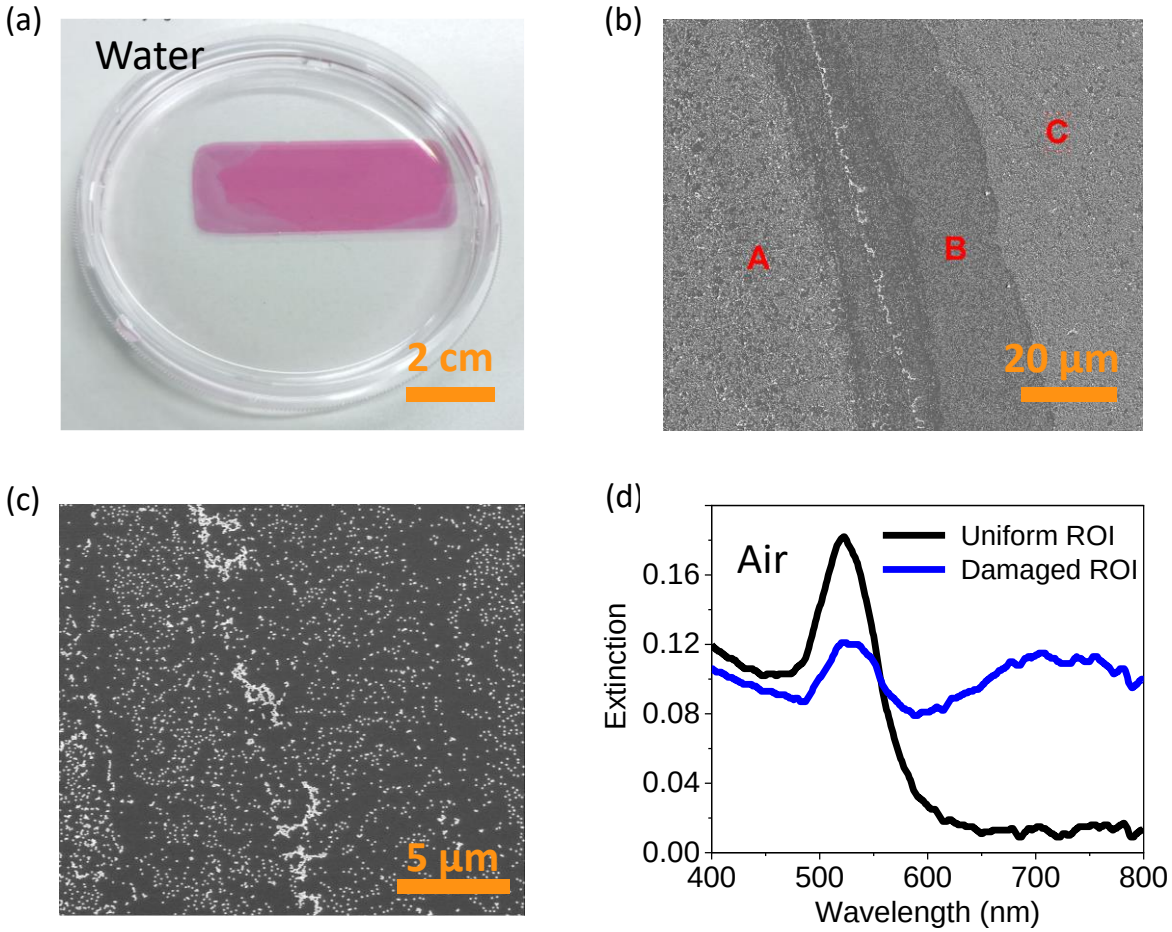

Figure S5. Effects of unproper drying of a AuNCs metasurface. (a) Photograph of the metasurface showing visible alterations occurred at the water-air interface during its remotion from the petri dish after the rinsing step by ultrapure water. The metasurface is in ultrapure water. (b) STEM micrograph of a damaged area showing two uniform sub-ROIs, labelled as "A" and "C", and a non-uniform sub-ROI, labelled as "B". (c) STEM micrograph at higher magnification of sub-ROI B, showing areas of NP depletion and accumulation. (d) Experimental extinction spectra of a uniform ROI (black) and a damaged ROI (blue) of the metasurface shown in (a). The blue spectrum exhibits a typical secondary shoulder associated with NP clusters. Note that the LSPR maximum of the black spectrum is lower than the one reported in Figure 2g of the Main since the OD of the AuNCs colloid used in this experiment was lower (OD 3.5 rather than OD 5).

S6. NND distributions of AuNSs and AuNCs metasurfaces

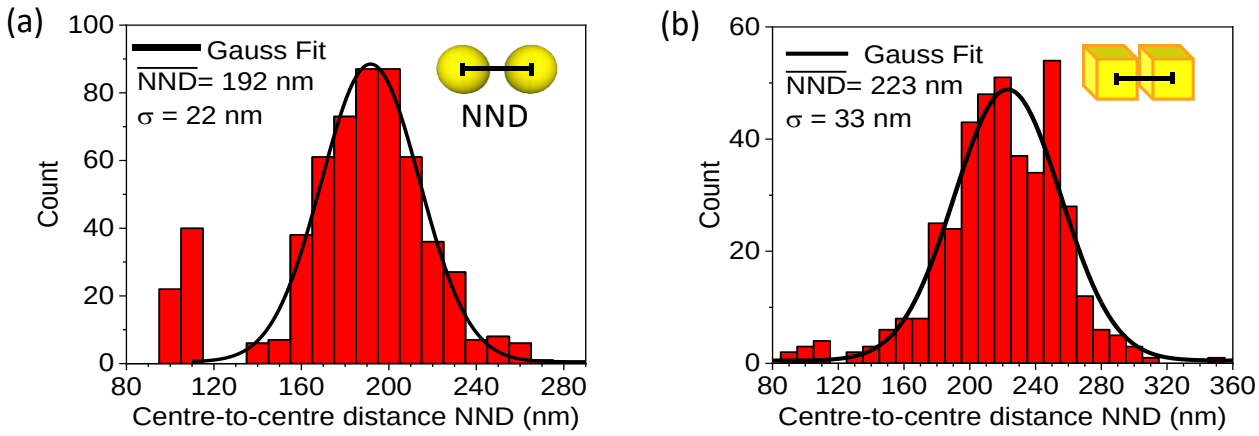

Figure S6. Nearest-neighbor center-to-center distances (NND) distributions for: (a) the AuNSs metasurfaces displayed in Figure 2b of the Main; (b) the AuNCs metasurface displayed in Figure 2f of the Main. The first two bins in (a) and the first three bins of (b) count NPs forming clusters while all other bins count NPs that are well-separated from each other.

S7. Processing and modelling of STEM micrographs (AuNCs case)

After the initial binarization and segmentation, the "Oriented Bounding Box" tool from "MorphoLibJ" plugin was used to extract center coordinates ($X_{n,c}$, $Y_{n,c}$), length L_n^* width W_n^*, and orientation α_n of the box bounding each n-th NC within the chosen region of interest (ROI) (in this case, the STEM micrograph in Figure 1d of the Main). By default, $L_n^* > W_n^*$ and the box orientation α_n is the angle between the x-axis and L_n^*. Instead, the NCs heights H_n^* were unknown due to the 2D nature of STEM micrographs. However, 52°-tilted STEM micrographs (see Figure 1e of the Main) showed AuNCs having randomly distributed heights rather than being at the

Figure S7. Processing and modelling of a STEM micrograph of a AuNCs metasurface. (a) Processed STEM micrograph at high magnification. An oriented bounding box is associated to each NP as a result of the "oriented bounding box" plugin. (b) Top-view of the corresponding model in Lumerical workspace obtained considering the parameter vectors $\boldsymbol{V_n^*}$. (c) Overlap of (a) and (b), to emphasize the faithful reproduction of the ROI morphology by the modelling.

same level. To capture this general feature, we set the heights as $H_n^* = (L_n^* + W_n^*)/2$. The $Z_{n,c}^*$ coordinate of each box centre was then calculated as $Z_{n,c}^* = H_n^*/2 + h$ with respect to the substrate level h^* set as $h^* = -\max(H_1^*/2, \dots, H_n^*/2, \dots)$. It is worth recalling that our AuNCs are not ideal cubes/parallelepipeds; rather, their edges and corners are rounded. The morphological and optical analysis reported in the Result section of the Main provided $\bar{R} = 14$

nm as the best radius of curvature to optically describe the round features of the NCs. Therefore, each visible AuNC in the micrograph could be modelled as the "all-rounded quadrilateral" object from Lumerical's object library (a parallelepiped with all edges and corners rounded by suitable cylinders and spheres, respectively) through the vector $\boldsymbol{V_n^*} = \left(X_{n,c}, Y_{n,c}, Z_{n,c}^*, L_n^*, W_n^*, H_n^*, \alpha_n, \bar{R}\right)$. Figure S11b displays the top-view of the as-obtained model associated to the processed STEM micrograph of Figure S11a. The visible ROI morphology is reproduced with exceptional precision as demonstrated by Figure S11c, which is the superposition of Figures S11a and S11b. It is worth mentioning again (see section S4) that the "oriented bounding box" outcomes $L_n^*,\ W_n^*$ are slight overestimations of length and width of the visible rectangular object. The overestimation could be easily evaluated after comparison with "manual" measurements. In the case of the micrograph of Figure S10a (magnification: 250'000x, 0.865 pixel/nm), the overestimations of L_n^*, W_n^* were found to be within 3 nm (1-3 pixels). Furthermore, the visible objects are enclosed into a 6 nm thick sputtering layer (see section S3). It follows that the best estimations for the real length L_n and width W_n of a NC are $L_n = L_n^* - (3 + 12)$ nm and $W_n = W_n^* - (3 + 12)$ nm. Consequently, the best estimation for the height is $H_n = (L_n + W_n)/2$ and then $Z_{n,c} = H_n/2 + h$ with $h = -\max\left(H_1/2, \dots, H_n/2, \dots\right)$. In conclusion, $\boldsymbol{V_n} = \left(X_{n,c}, Y_{n,c}, Z_{n,c}, L_n, W_n, H_n, \alpha_n, \bar{R}\right)$ was the final vector that we considered for each visible NC to take into account both the processing artifacts and the sputtering layer.

References

1 M. N. O'Brien, M. R. Jones, K. A. Brown and C. A. Mirkin, *J. Am. Chem. Soc.*, 2014, **136**, 7603–7606.

2 B. Nikoobakht and M. A. El-Sayed, *Chem. Mater.*, 2003, **15**, 1957–1962.

3 J. Rodríguez-Fernández, J. Pérez-Juste, P. Mulvaney and L. M. Liz-Marzán, *J. Phys. Chem. B*, 2005, **109**, 14257–14261.

4 J. E. Millstone, W. Wei, M. R. Jones, H. Yoo and C. A. Mirkin, *Nano Lett.*, 2008, **8**, 2526–2529.

5 W. Niu, S. Zheng, D. Wang, X. Liu, H. Li, S. Han, J. Chen, Z. Tang and G. Xu, *J. Am. Chem. Soc.*, 2009, **131**, 697–703.

6 W. Li, M. Zhang, J. Zhang and Y. Han, *Front. Chem. China*, 2006, **1**, 438–442.

7 K. Park, H. Koerner and R. A. Vaia, *Nano Lett.*, 2010, **10**, 1433–1439.

8 C. Wang, C. Siu, J. Zhang and J. Fang, *Nano Res.*, 2015, **8**, 2445–2466.

9 D. J. Schupp, J. Angst, E. A. Schaefer, S. M. Schupp and H. Cölfen, *J. Phys. Chem. C*, 2021, **125**, 20343–20350.

10 C.-J. Huang, P.-H. Chiu, Y.-H. Wang, W. R. Chen and T. H. Meen, *J. Electrochem. Soc.*, 2006, **153**, D129.